

Forecasting Challenges Associated With Tropical Cyclones Within Subtropical Gyres

BRIAN CRANDALL, JOHN MOLINARI AND DAVID VOLLARO

Department of Atmospheric and Environmental Sciences, University at Albany,
State University of New York, Albany, New York

Submitted to *Weather and Forecasting*

April 26, 2013

Revised August 21, 2013

Final revision September 26, 2013

Corresponding author address:

John Molinari

University at Albany, SUNY

Atmospheric and Environmental Sciences, ES 351

1400 Washington Avenue

Albany, NY 12222

ABSTRACT

This case study examines the complex history of a tropical storm that formed southeast of a large subtropical gyre. In real time the tropical storm was incorrectly identified as being two separate storms, and at one time was mislocated by 465 km. The unique forecast problems associated with tropical cyclones within a subtropical gyre are described.

The tropical storm propagated around the gyre and encountered a midlevel temperature gradient to the north. The interaction of the storm with this gradient produced a strong midtropospheric temperature dipole. Temperature advection within this feature produced a change in structure to a subtropical storm co-rotating with an upper low. The subtropical storm turned equatorward and nearly came to a halt as the upper low became aligned with the storm. As convection increased over warm water, the upper low shifted away from the center and the storm reversed direction and moved poleward. These sudden track changes have frequently been observed in the northwest Pacific, but the role of midtropospheric temperature gradients has not previously been addressed.

Clear air at the gyre center coincided with a region of cold advection. A fishhook structure in the gyre cloudiness developed as a result of warm advection east and north of the gyre. The subtropical structure of the storm evolved within the fishhook. It is recommended that JTWC provide formal warnings on subtropical storms, because their baroclinic nature can produce dramatic track changes associated with the presence of upper lows near the center.

1. Introduction

The western north Pacific plays host to a variety of synoptic-scale meteorological phenomena during the boreal summer. The origins of these events range from the tropical latitudes through the subtropics and into the extratropical activity of the mid-latitudes. One such phenomenon is a large low-pressure area that encompasses a sizable fraction of the subtropical Pacific. While its presence is not unusual, there is no established nomenclature to describe the feature. Holland (1995) describes it as “a monsoon depression”, while Harr et al. (1996) and Carr and Elsberry (1995) use the term “monsoon cyclone”, and Lander (1994, 1996), Chen et al. (2004), Molinari et al. (2007), and Wu et al. (2013a) label it a “monsoon gyre”. Molinari and Vollaro (2012) call the feature a “subtropical gyre”, referencing its location in the subtropical latitudes, 1000 km north of the latitude of the long-term monthly mean axis of the monsoon trough (Lander 1994; Molinari et al. 2013). The term “subtropical gyre” is used here.

Subtropical gyres have distinct characteristics that make them unique among western north Pacific disturbances. While the gyre center is often devoid of cloud cover, extensive and deep convection exists on its equatorward and eastward sides (Lander 1994; Molinari et al. 2007; Molinari and Vollaro 2012). The description of gyre duration and rate of occurrence varies widely. Lander (1994) suggests that gyres have a life span approximately two to three weeks, and develop once every other year on average. Chen et al. (2004) defined a gyre as having a lifespan of 5 days or greater and concluded gyres occur 6 times per year. Recently Wu et al. (2013a) found a gyre frequency of 3.4 per year, and lifespans ranging from 4 to 17 days.

Several papers describe the relationship between gyres and tropical cyclones (TCs). Holland (1995) hypothesized that TCs develop from small surface vortices formed within the mesoscale convective systems (MCSs) of the subtropical gyre. Lander (1994) noted that small TCs (less than 1° in size; Brand 1972) can develop in the eastern quadrant of the subtropical gyre

and rotate cyclonically within the gyre circulation before they separate and move independently. Giant TCs (greater than 10° longitude in size; Brand 1972) may form if the center of the gyre itself acquires deep convection. Wu et al. (2013a) found that 42 TCs formed within the 37 subtropical gyres they studied during the months of May-October 2000-2010, representing almost 20% of all TCs that formed during the period. Gyre-based TCs peaked in frequency during August and September.

Carr and Elsberry (1995) examined sudden track changes in WNP TCs. They defined these as “a rapid slowing of the westward movement to either a quasi-stationary or tight cyclonic looping period and then a strong acceleration on a substantially more poleward heading”. They recorded an average of 2-3 sudden track changes per year in JTWC data from 1977-1991. Carr and Elsberry (1995) used a nondivergent barotropic model to simulate the presence of a large gyre with an embedded TC to its southeast and reproduced a rotation of the TC around the gyre, followed by a slowing of forward motion and then a northward turn. They thus argued that binary interaction between the gyre and the TC could produce sudden track changes to the north or northwest. Wu et al. (2011; 2013b) made similar arguments. None of these papers addressed the possible role of middle latitude interactions and upper tropospheric lows and baroclinic effects in sudden track changes in the vicinity of gyres. Middle latitude lows frequently reach the subtropics during gyre formation and evolution (Lander 1994; Holland 1995; Molinari et al. 2007; Molinari and Vollaro 2012).

In summary, there is ample evidence that subtropical gyres influence TC formation and motion as well as the accuracy of TC forecasts. Furthermore, because the subtropical gyre itself creates substantial convection and strong surface winds (Lander 1994), it can be difficult to identify TCs within the gyre. This work examines a case of a tropical storm forming within the

circulation of a subtropical gyre in July 1989. The circumstances of this case are unusual. In real time two tropical storms (Ken and Lola) were named; in JTWC post-season analysis, the two were found to be the same storm. In addition, the storm was mislocated at one particular observation time by 465 km. During the storm history discussion the storms will be labeled Ken and Lola, but otherwise the label Ken-Lola will be given to the single storm. The motivation for this work is to understand what circumstances were responsible for such dramatic real-time errors. We will show that the nature of the gyre background flow and substantial interactions with a midlatitude baroclinic zone played critical roles in the forecast challenges with the storm. Particular problems that arise in forecasting TCs within subtropical gyres will be addressed.

2. Data and Methods

2.1 Data Sources

ERA-Interim gridded analyses (Simmons et al. 2007; source website: www.ecmwf.int/products/data) from the European Center for Medium Range Weather Forecasting Operational (ECMWF) interpolated to a 1.125° latitude-longitude resolution and available four times daily were used to obtain values for the wind, height, temperature, relative humidity, and vorticity fields. Convective activity was evaluated using infrared brightness temperature data from the Cloud Archive User Service (CLAUS), available on a 0.5° latitude-longitude grid eight times daily. Satellite imagery was supplied by the JMA GMS-3 satellite, and downloaded from the NCDC Gridsat-B1 CDR satellite imagery archive (<http://www.ncdc.noaa.gov/oa/gridsat/index.php?name=CDR>). JTWC TC track and intensity data were obtained from the NOAA IBTrACS database (<http://www.ncdc.noaa.gov/oa/ibtracs/index.php?name=ibtracs-data>). Only time periods where

the TC reached tropical storm intensity or greater are used in this work. Sea surface temperature (SST) came from the NOAA Optimum Interpolation V2 analyses (<http://www.cdc.noaa.gov/>).

Vertical wind shear is calculated as the vector difference between the mean winds at 200 and 850 hPa over 500 km of radius of the storm center using ERA Interim gridded analyses. Because Cartesian components are averaged to produce the mean winds, the mean vortex is automatically removed. This calculation provides a measure of the ambient wind shear rather than that near the storm core, but this measure has been shown to account for the observed asymmetries in convection in storms (e.g., Corbosiero and Molinari 2003). Ambient shear estimates from global models come surprisingly close to those based on a near-core vertical wind shear in the few available studies (Eastin et al. 2006; Braun et al. 2006; Reasor et al. 2009). Mean wind between 1000 and 200 hPa, a measure of TC steering flow, was also calculated over 500 km of radius from the same gridded analyses.

2.2 Definitions

To understand the development of TCs within the subtropical gyre environment, the gyre needs to be defined. The definition used by Lander (1994) and Holland (1995) is largely subjective, with no clear delineation between when a large subtropical low is or is not a gyre. Chen et al. (2004) used 5 criteria in their gyre definition: (a) a closed circulation more than 2500 km in width on an 850 hPa streamline map; (b) deep convection to the south-southeast of the core; (c) separation of the low from continental lows over east Asia, and the presence of adjacent anticyclones to the SSW and ENE; (d) a weak ridge above the gyre; and (e) a sequence of small vortices forming along the SSE edge. Each of these was evaluated subjectively. Wu et al. (2013a) defined gyres by first filtering out tropical cyclones and then using 10-day lowpass-

filtered 850 hPa winds. The gyre in the filtered winds had to be visually greater than 2500 km in diameter and contain substantial convection south or southeast of its center.

Both of the above definitions have subjective aspects, and an objective definition was preferred. In order for the definition to be usable in real time, no time filtering was carried out. Details such as the presence of ridges and troughs in certain locations were removed for simplicity and objectivity. The two criteria for defining a gyre in this paper require only the existence of a huge cyclonic circulation of sufficient strength:

- (1) The azimuthally-averaged circulation at 850 hPa must remain cyclonic in each 100-km radial bin from the center to a radius of 2000 km. Since $\overline{C} = 2\pi r \overline{v_\lambda}$, this means the azimuthally-averaged tangential wind at 850 hPa must remain positive for that radial range.
- (2) The azimuthally-averaged tangential wind speed at 850 hPa must reach at least 8 m s^{-1} at some radius within the circulation.

The first criterion eliminates individual tropical cyclones (e.g., see Fig. 3 from Molinari and Vollaro 2012), except those that form near the center of an already existing gyre. The second criterion eliminates the kind of broad weak cyclonic flow that can accompany, for instance, the monsoon trough of the northwest Pacific. This definition omits a minimum temporal requirement and defines the lifespan of the subtropical gyre as the time period where it fulfills both conditions.

It will be seen that tropical cyclones forming within gyres have atypical convective signatures and will sometimes have characteristics of subtropical storms. Such storms are defined by the U.S. National Hurricane Center (NHC; J. Franklin, personal communication, 2013) as “non-frontal, synoptic-scale cyclones that originate over tropical or subtropical waters,

and have a closed surface wind circulation about a well-defined center. In addition, they have organized moderate to deep convection, but lack a central dense overcast. Unlike tropical cyclones, subtropical cyclones derive a significant proportion of their energy from baroclinic sources, and are generally cold-core in the upper troposphere, often being associated with an upper-level low or trough.” A tropical cyclone with such characteristics will be shown in this study.

3. Analysis of Tropical Storm Ken-Lola

3.1 Storm History

Table 1 gives a brief chronology of major events and warnings issued by JTWC regarding the formation and decay of Ken and Lola in real time. Table 2 examines the maximum wind speeds in the storms, the ambient 850-200 hPa vertical wind shear direction and magnitude, the mean SST within 1 degree latitude and longitude of the storm center, and the mean wind 1000-200 hPa. The history of Ken and Lola is further described in Fig. 1, which displays IR satellite imagery overlaid with surface wind observations from coastal stations, ships and buoys every six hours from 0000 UTC 29 July to 1800 UTC 31 July. Fig. 1 also displays the post-season track of Ken-Lola determined by JTWC. The tropical cyclone symbol shows the best track location at each time.

A gyre had already formed during 28 July (Crandall 2012). The gyre formation was tied directly to interactions with midlatitude upper tropospheric troughs (Crandall 2012) in a manner similar to that shown by Molinari and Vollaro (2012), and is not addressed in this paper. By 0000 UTC 29 July (Fig. 1a), the gyre is visible as a broad circulation with cloudiness primarily to its south and east. A closed circulation was centered on the edge of the broad gyre cloudiness

to the south. This will be referred to as the pre-Ken circulation. Six hours later (Fig. 1b), this circulation persisted on the inner edge of the larger envelope of convection associated with the subtropical gyre. Analysis of synoptic data and satellite imagery led to the issuance of a Tropical Cyclone Formation Alert (TCFA) at 0930 UTC 29 July, and it was noted by the JTWC that active convection was displaced well to the south of the center. This convective asymmetry was consistent with what is expected from the northerly ambient vertical wind shear (i.e., downshear convection; see Corbosiero and Molinari 2003). By 1200 UTC (Fig. 1c), the organization of the pre-Ken disturbance had improved, as deep convection developed near its center. As the disturbance traveled around the gyre (Fig. 1d, 1800 UTC 29 July), convection flared up south of the center (again downshear), and gale force winds were observed by ships near the center. By 0000 UTC 30 July (Fig. 1e), a circular mass of clouds was present near the center of the pre-Ken disturbance, bearing similarities to the “midget TCs” in subtropical gyres described by Lander (1994). The mean wind (Table 2) around the storm turned more southerly as the storm moved to the east side of the gyre.

The broad area of gale-force winds at 0000 UTC 30 July well to the north of the pre-Ken circulation represents a striking and unexpected feature. It was accompanied by a westward extension of cloudiness north of the broad gyre, resembling the start of a “fishhook” pattern described by Lander (1996). It will be shown later that these gale-force winds are linked to a separate vorticity maximum ahead of the soon-to-be TC.

The pre-Ken circulation was first declared Tropical Depression 13W at 0400 UTC 30 July. At 0900 UTC 30 July, in the presence of continuing moderate vertical wind shear, the JTWC determined that the depression reached tropical storm intensity, becoming Tropical Storm (TS) Ken, applied retroactively to 0600 UTC. At that time (Fig. 1f), the system took on the

appearance of a small TC. JTWC reported maximum sustained winds of 45 kt (23 m s^{-1}). Fig. 1f shows the presence of clear air at the center of the gyre immediately to the west of the TC as the storm continued to move along the inner edge of gyre cloudiness. A separate area of strong gales persisted well to the north of TS Ken. These gales existed in the same region that clouds were extending westward north of the gyre, further defining the fishhook pattern described previously.

By 1200 UTC 30 July (Fig. 1g), TS Ken developed a more diffuse structure as it moved over cooler water and vertical wind shear slowly increased (Table 2). Tropospheric mean flow developed a component from the east as the TC continued its path around the larger gyre. Gales to the north continued under the developing clouds extending westward north of the gyre. As TS Ken moved northwestward into the northern flank of the gyre circulation at 1800 UTC 30 July (Fig. 1h), high clouds within the TC were restricted to a small convective maximum north of the center. As shown in Table 2, vertical shear continued to increase from the south-southwest. Meanwhile, the fishhook structure north of the gyre continued to extend westward, and was accompanied by a well-defined surface cyclonic circulation.

Vertical wind shear continued to increase at 0000 UTC 31 July (Table 2). Virtually no deep convection existed within the vicinity of TS Ken (Fig. 1i). At this time two decisions were made in real time that turned out to be erroneous. First, the real-time location of Ken was placed 465 km southeast of the post-season position shown in Fig. 1i, within the convective region on the eastern edge of the gyre. The magnitude of this error would be equivalent to locating a storm near Jacksonville, FL when it was actually east of Wilmington, NC. Second, the last warning was issued at this time on Ken, ending its lifetime. However, a visible satellite image only 25 minutes later from Fig. 3-13-2 of the post-season JTWC report

(<http://www.usno.navy.mil/NOOC/nmfc-ph/RSS/jtwc/atcr/1989atcr.pdf>) showed a classic

sheared tropical storm with a central swirl of low clouds. Cloudiness existed downshear and downshear-left (north and northwest of the center, consistent with shear from the southwest in Table 2). These clouds do not show well on the infrared images in Fig. 1, likely because cloud-top heights were too low. The end of warnings on TS Ken, at a time when a sheared tropical cyclone was still clearly shown on visible satellite images, would soon have consequences. Indeed, after the season JTWC stated the following: “A detailed post-analysis, even though not absolutely conclusive, strongly suggested that Tropical Storms Ken and Lola were probably the same system”.

Six hours later, at 0600 UTC 31 July, a TCFA was issued for a new disturbance that was west of the TS Ken position 6 h earlier. This disturbance shows clearly in the surface wind field in Fig. 1j, located within clouds associated with the fishhook north of the gyre. Vertical wind shear was decreasing and underlying SST was rising (Table 2). Using 0300 UTC reports of 50 kt (26 m s^{-1}) winds from the USS *Dubuque* (LPD8), and 0600 UTC reports from the same ship of 40 kt winds and falling surface pressures, the decision was made to issue warnings for TS Lola at 1030 UTC 31 July. In reality, as noted in the JTWC post-season report, these winds were associated with the same disturbance that was previously labeled TS Ken. By 1200 UTC 31 July (Fig. 1k), TS Lola had an asymmetric cloud structure, but a well-defined circulation with high clouds rotating to the south of the center. Mean flow had turned to the northeast, vertical shear remained moderate, and SST continued to rise as the storm turned toward the southwest. At the last time period shown, 1800 UTC 31 July (Fig. 1l), the highest clouds had rotated around to the east of Lola. Mean flow remained from the northeast but weakened. The remainder of this section will examine other fields, largely using gridded ERA Interim analyses, in order to

understand the evolution of the background flow that created such a complex evolution of TS Ken-Lola.

Fig. 2 shows the 850 hPa relative vorticity and winds daily at 0000 UTC from 29 July, just before Ken was named, to 1 August, after Lola had formed. Only cyclonic vorticity is shaded, starting at $5 \times 10^{-5} \text{ s}^{-1}$, in units of $5 \times 10^{-5} \text{ s}^{-1}$. At 0000 UTC 29 July (Fig. 2a), the broad gyre shows clearly in the wind and cloud fields. One vorticity maximum (“A”) was present south of the gyre center at the location of the pre-Ken disturbance shown in Fig. 1a. A second vorticity maximum (“B”) was found northeast of the gyre center, adjacent to the extended cloudiness to the east. One day later (Fig. 2b), both vorticity maxima rotated around the broader gyre and approached one another. Disturbance A was associated with the pre-Ken disturbance. Disturbance B was present just south of the gale force wind region shown in Fig. 1e. By 0000 UTC 31 July (Fig. 2c), the two vorticity maxima merged into one elongated maximum along the inner edge of cloudiness north of the gyre. The primary maximum (A) was co-located with the tropical storm, but an extended maximum to the west (B) lay almost directly under the upper clouds within the fishhook. As a result, there is still some evidence at this time of two vorticity maxima. By 0000 UTC 1 August, the high clouds with TS Lola broke away from the broad gyre cloudiness and a single strong vorticity maximum existed at 850 hPa, coincident with the tropical cyclone. The broad gyre cloudiness and wind field continued to show prominently at this last time, and another 850 hPa vorticity maximum rotated around the gyre to the east. The latter was not associated with subsequent tropical storm development.

Fig. 3 provides some insight into the structure of the gyre. It displays temperature and wind at 500 hPa over the same infrared images as Fig. 2. A considerable north-south temperature gradient existed. Cold advection, indicated by winds crossing isotherms toward warmer air, was

present north of the gyre center from 25-30°N and 130-135°E (Fig. 3a). By quasi-geostrophic reasoning this region would be expected to exhibit subsidence, and it is indeed accompanied by clear air. In contrast, warm advection was present east of the gyre. This region of warm advection lined up well with the observed cloudiness in the same region. Temperature advection was near zero south of the gyre. The cloudiness in that region was most likely associated not with baroclinic effects, but with enhanced surface fluxes in the strong surface westerlies south of the gyre (Fig. 1), consistent with the results of Molinari and Vollaro (2012).

By 0000 UTC 30 July (Fig. 3b), TS Ken had formed. Cold advection and clear air continued at the center of the gyre. The development of the fishhook pattern in the clouds was associated with a westward extension of warm advection north of the gyre. By 0000 UTC 31 July (Fig. 3c), TS Ken had moved into the pre-existing midtropospheric temperature gradient. The northerly flow ahead of Ken brought cold air equatorward, creating a dipole of small-scale warm and cold centers. Once again the clear region in the center of the large gyre coincided with the region of cold advection, and the expanding fishhook was directly associated with warm advection. By 0000 UTC 1 August (Fig. 3d), the temperature dipole had rotated cyclonically, so that the cold air now was northeast of the center and the warm air to the southwest. The asymmetric cloudiness associated with Ken-Lola rotated as well. Cloudiness existed at the azimuths of warm advection in the storm, while the less cloudy side of the storm exhibited cold advection. Fig. 3 indicates that the evolution of cloudiness in both the gyre and the later stages of Ken-Lola were tightly coupled to the midlevel temperature advection field.

Fig. 4 shows 200 hPa height fields for the same times as Figs. 2-3. A westward moving upper low comprised the dominant feature at this level during the period. At 0000 UTC 29 July (Fig. 4a), the upper low produced northerly flow into the center of the gyre, and southerly flow

within the clouds east of the gyre. The low was northwest of the 500 hPa circulation, consistent using thermal wind reasoning with the temperature gradient at 500 hPa in Fig 3. The upper low was nearly coincident with 850 hPa vorticity maximum B. The track of TS Ken had to be more influenced by the deep circulation of the gyre than the shallower upper tropospheric trough. As a result, by 0000 UTC 31 July (Fig. 4c) TS Ken moved closer to the upper low as it moved around the gyre. The proximity of the storm to the upper low is consistent (using thermal wind reasoning) with the strong temperature dipole at this time at 500 hPa (Fig. 3c). By 0000 UTC 1 August (Fig. 4d), the upper low had rotated around to northeast of TS Ken-Lola, following the path of the midlevel temperature dipole (Fig. 3d).

Fig. 5 displays 500 hPa relative humidity (RH). High humidity, defined as $RH > 60\%$, is shown with yellow stippling, and low humidity ($RH < 40\%$) with blue stippling. In general, the relative humidity field north and east of the gyre is associated with quasi-geostrophic forcing of vertical motion by temperature advection. At 0000 UTC 29-30 July (Fig. 5ab), dry air corresponds to cold advection north of the gyre, while moist air is present in the regions of warm advection to the east. The extension of high relative humidity to the west in the fishhook corresponds to the warm advection region. At 0000 UTC 31 July (Fig. 5c), dry air wrapped in behind TS Ken, while moist air was drawn southward in the fishhook cloud pattern west of TS Ken. At the final time, a smaller-scale dipole of moisture was once again dynamically consistent with the temperature advection pattern. South of the gyre, relative humidity remained large throughout the period.

Figs. 1-5 suggest that the motion, intensity, and structure of TS Ken were influenced by the broad gyre. First, the storm was carried northward, then westward, by the gyre circulation, as shown in Figs. 1-2. This motion brought TS Ken over a region of cooler SST, which produced a

less organized cloud field and the near elimination of high cloud close to the storm center. Shortly thereafter, gyre-induced westward motion brought TS Ken into a region of meridional temperature gradient in the midtroposphere. This resulted in a strong tropical storm-scale dipole in the midlevel temperature, which by thermal wind reasoning was associated with an upper low over the cold pool west of the storm. Subsequently this temperature dipole and the related upper tropospheric low appeared to co-rotate with the tropical storm. This interaction produced a cyclonic turning and a slowing of the forward motion of Ken-Lola. In addition, it produced a pattern of warm and cold advection that closely followed the cloud asymmetry in the storm, with clouds in the area of warm advection. The development of this latter subtropical storm structure will be addressed in the following section.

3.2 Evolution of Ken-Lola into a Subtropical Storm

Fig. 6 shows the evolution of the location of the 1000 hPa (red) and 200 hPa (blue) height minima with respect to the midpoint between them, following the procedures of Holland and Lander (1993). The plot covers from 1200 UTC 29 July to 0000 UTC 1 August, every 6 hours. Because range rings represent the distance from the midpoint, the actual distance between the 1000 and 200 hPa lows is double the range ring value. On 29 July, TS Ken approached the upper low. On 30 July TS Ken moved northward around the gyre as the upper low moved westward. On 31 July, the storm and the upper low became tightly coupled and approached one another, consistent with Fig. 4. It was on this day that Ken-Lola began to take on subtropical characteristics. Fig. 7 shows six-hourly 500 hPa temperature and wind on 31 July. The evolution of the fishhook pattern in the clouds was tied directly to the temperature advection pattern as the warm advection region propagated completely around the tropical storm over 24 h. Using the

NHC definition of subtropical storms given in Section 2.2, several subtropical characteristics of Ken-Lola were apparent: a closed circulation with tropical-storm force winds about a well-defined center (Fig. 1i-l); moderate to deep convection near the center, but no central dense overcast; a baroclinic structure, with temperature gradients in the midtroposphere that are consistent with the cloud asymmetry (Fig. 7); and an upper low close to the center (Fig. 4c), unlike ordinary tropical cyclones that contain upper tropospheric anticyclones. As of this writing, JTWC does not formally warn on subtropical cyclones. There might be value in doing so, because the presence of the upper trough produced an unusual tropical cyclone track, as will be described in the following section.

3.3 Dramatic track changes in TS Ken-Lola

Fig. 1 showed the full track of TS Ken-Lola. This track contained several striking aspects: (i) the storm traveled in almost a full circle as it rotated around the gyre; (ii) on 30 July the storm moved equatorward and virtually came to a stop as the mean wind fell to nearly zero (Table 2); and (iii) the storm then turned northward and westward. This motion closely fits the sudden track changes of western north Pacific storms described by Carr and Elsberry (1995). Fig. 7 showed the reasons for the turn southward and the nearly stationary period: the storm became tightly coupled to and co-rotated with an upper low, which ended up vertically aligned. The upper low evolved as a result of the small-scale rotating temperature dipole in the midtroposphere produced by the motion of Ken-Lola into a strong meridional temperature gradient.

The reasons for the subsequent northwestward motion on 2-3 August can be seen in Fig. 8. It shows 500 hPa temperature and wind (top panels) and 200 hPa height and wind (lower panels), at 0000 UTC 2-3 August. At 0000 UTC 2 August (Fig. 8a), the 500 hPa temperature

continues to show cold and warm anomalies rotating about the center of Ken-Lola, with clouds present in the region of warm advection as before. The cold pool was further from the center than earlier (compare to Fig 3d). As a result, the upper tropospheric low (Fig. 8c) lay farther northwest of the tropical storm. By 0000 UTC 3 August, the region of warmest 500 hPa temperature (Fig. 8b) moved almost over the center of Ken-Lola. We hypothesize this was a result of stronger core convection warming the column. As a consequence, the cold air and the upper low shifted southwest of the center. This resulted in a mean flow from the southeast that accelerated the storm poleward after the nearly stationary period (see mean flow evolution in Table 2). Ken-Lola continued to develop more tropical characteristics again as it moved northwestward toward landfall in China (not shown). Ken-Lola thus experienced a complex history as a midlevel TS (Lander 1994) that became sheared, encountered a midlatitude temperature gradient where it developed subtropical characteristics, moved equatorward, then poleward, and returned to a more symmetric tropical storm as it experienced renewed core convection.

4. Discussion

4.1 Gyre Structure

The subtropical gyre in this case exhibited characteristics that have been described previously by Lander (1994), Chen et al. (2004), Molinari et al. (2007), Molinari and Vollaro (2012), and Wu et al. (2013a). The center of the gyre was largely clear, while an extensive region of cloudiness extended from south to east of the gyre center. The gyre exceeded 4000 km in diameter (not shown; see Crandall 2012) for several days, the same as found for a 1988 gyre by Molinari and Vollaro (2012). The gyre contained multiple vorticity maxima over several days, three of which were shown in this paper. A small tropical cyclone formed south of the gyre

center and moved around the gyre, a common behavior (Lander 1994). A “fishhook” structure in the cloud field (Lander 1994) developed as cloudiness extended westward, then southward, north of the gyre.

The role of midtropospheric temperature gradients in the above behavior was examined. The clouds east of the gyre and the developing fishhook were directly associated with warm advection at 500 hPa, and also at 300 hPa (not shown). This warm advection occurred in part as the gyre circulation acted on the background meridional temperature gradient, but was enhanced by the role of the TC (see following section). In addition, the clear region at the center of the gyre coincided with midlevel cold advection and thus dynamically induced subsidence. The importance of quasi-geostrophic dynamics and pre-existing meridional temperature gradients in gyre structure and evolution has not previously been shown. In contrast, temperature advection south of the gyre was small and often negative. The strong, deep convection south of the gyre was likely associated with strong surface fluxes in the enhanced westerlies, consistent with the results of Molinari and Vollaro (2012).

4.2 Role of the gyre in the evolution of Ken-Lola

Figure 9 shows a schematic depiction of the history of Ken-Lola over a plot of SST averaged from 27 July – 2 August. The large subtropical gyre played several important roles in the evolution of Ken-Lola. First, as seen from the track in Fig. 9 and the mean flow evolution in Table 2, the gyre provided the background flow that carried TS Ken poleward and then westward. As Ken moved poleward, it encountered cooler water (Fig. 9) and weakened. As it continued westward around the gyre, it encountered a strong midlevel temperature gradient (Fig. 7). An intense, small-scale temperature dipole arose as Ken-Lola transported cold air southward ahead of its path. This dipole produced subtropical characteristics in the storm, with asymmetric

convection associated with warm advection at middle levels. Ken-Lola fit the NHC definition of a subtropical storm: tropical-storm force winds about a well-defined center (Fig. 1i-l); moderate to deep convection near the center, but no central dense overcast; a baroclinic structure, with temperature gradients in the midtroposphere consistent with the cloud asymmetry (Fig. 7); and an upper level low very close to the center (Fig. 4). The interaction of Ken-Lola with the upper tropospheric low produced a cyclonic turning of the storm back toward the equator. The storm then encountered higher SST and smaller vertical wind shear (Table 2). As Ken-Lola and the upper low became almost coincident, the storm became nearly stationary for 24 h. Thereafter, the convective signature at the storm center became stronger and more symmetric, the midlevel warm anomaly shifted to nearly over the center, the colder air shifted southwestward, and mean flow carried the storm toward the northwest.

This explanation for a sudden northward track change differs from those of Carr and Elberry (1995) and Wu et al. (2013b), who attributed such track changes to interactions between the gyre and the TC. Although that process might play a role in the Ken-Lola track, the evidence from Fig. 8 suggests that the upper low was a major factor. Because the small scale of the upper low was connected dynamically to the midlevel temperature gradient, the latter appears to be critical for sudden track changes as well as for the subtropical storm structure. These upper level phenomena were not considered by previous researchers. The presence of the gyre background flow, including the strong temperature gradient, was responsible for most of the unexpected behavior of Ken-Lola.

4.3 Challenges in Forecasting Gyre-Based TCs

The case examined in this paper took place before the characteristics of subtropical gyres were recognized (Lander 1994). JTWC now attempts to identify gyres in real time. Many

complications produced by subtropical gyres have been covered by Lander (1994): the TCs are tiny and thus sensitive to vertical wind shear and SST changes; multiple vorticity maxima develop within the gyre, but only some of those support TC formation; and the small TCs are difficult to separate from the gales produced by the gyre. In this paper we have identified several additional characteristics of gyres that create a complex background flow for TCs. First, considerable dry air in regions of cold advection existed north and west of the extended gyre-based cloudiness. TCs tend to propagate along the inner edge of clouds and thus are always close to the dry air. This makes the storms vulnerable to weakening if dry air reaches the storm core as a result of vertical wind shear. Second, the presence of strong midlevel temperature gradients north of the gyre center has several consequences: the TC carried northward by the gyre in this study encountered temperature gradients, developed subtropical structure, and interacted with these gradients in a manner shown in Figs. 3-4 and 7-8 that produced cyclonic turning, slowing, and then a track change toward the north and northwest.

Currently JTWC does not warn specifically on subtropical cyclones, though their presence is often noted in the significant tropical weather advisory (ABPW/ABIO products). It is recommended that such designation should be made more formal in the manner currently done by NHC. The potential value of such labeling is reflected in the dramatic track changes that can be associated with subtropical structure.

A number of questions remain. Among these are (i) the frequency of midlevel temperature gradients in the vicinity of subtropical gyres; (ii) the extent to which TCs within gyres take on subtropical storm characteristics; (iii) whether sudden northward TC track changes always arise in part due to co-rotation with upper lows. Ideally, as other instances of gyres are studied and the

development of TCs within their circulations becomes better understood, it will permit more accurate prognosis of these complicated events.

Acknowledgements: We gratefully acknowledge the input and suggestions of our SUNY Albany colleagues in the preparation of this work. We thank two anonymous reviewers for their well-reasoned comments. Gridded analyses from the ECMWF were obtained from NCAR, which is supported by the National Science Foundation (NSF). This work was supported by NSF grants ATM0839991 and AGS1249732.

REFERENCES

- Brand, S., 1972: Very large and very small typhoons of the western North Pacific Ocean. *J. Appl. Meteor.*, **9**, 433-441.
- Braun, S. A., M. T. Montgomery, and Z. Pu, 2006: High-resolution simulation of Hurricane Bonnie (1998). Part I: the organization of the eyewall vertical motion. *J. Atmos. Sci.*, **63**, 19-42.
- Carr, L. E., III, and R. L. Elsberry, 1995: Monsoon interactions leading to sudden tropical cyclone track changes. *Mon. Wea. Rev.*, **123**, 265-289.
- Chen, T.C., S.Y. Wang, M.-C. Yen, and W. A. Gallus Jr., 2004: Role of the monsoon gyre in the interannual variation of tropical cyclone formation over the western north Pacific. *Wea. Forecasting*, **19**, 776-785.
- Corbosiero, K.L., and J. Molinari, 2003: The relationship between storm motion, vertical wind shear, and convective asymmetries in tropical cyclones. *Journal of the Atmospheric Sciences*, **60**, 366-376.
- Crandall, B.: An analysis of the formation and evolution of the 1989 western north Pacific subtropical gyre. M.S. thesis, Dept. of Earth and Atmospheric Sciences, University at Albany, State University of New York, 91 pp.
- Davis, C.A., and L.F. Bosart, 2003a: Baroclinically induced tropical cyclogenesis. *Mon. Wea. Rev.*, **131**, 2730-2747.
- Davis, C.A., and L.F. Bosart, 2003b: The TT problem: Forecasting the tropical transition of cyclones. *Bull. Amer. Meteor. Soc.*, **85**, 1657-1662.
- Eastin, M. D., P. D. Reasor, D. S. Nolan, F. D. Marks Jr., and J. F. Gamache, 2006: Evolution of low-wavenumber vorticity during rapid intensification: A dual-Doppler analysis. Preprints,

27th Conf. on Hurricanes and Tropical Meteorology, Monterey, CA, Amer. Meteor. Soc.,
4B.6.

Guishard, M. P., J. L. Evans, and R. E. Hart, 2009: Atlantic subtropical storms. Part II:
Climatology. *J. Climate*, **22**, 3574–3594.

Harr, P. A., M. S. Kalafsky, and R. L. Elsberry, 1996: Environmental conditions prior to
formation of a midget tropical cyclone during TCM-93. *Mon. Wea. Rev.*, **124**, 1693–1710.

Holland, G.J., 1995. Scale interaction in the western Pacific monsoon. *Meteor. Atmos. Phys.*, **56**,
57-79.

Holland, G.J., and M.A. Lander, 1993: The meandering nature of tropical cyclone tracks. *J.*
Atmos. Sci., **50**, 1254-1266.

Knaff, J.A., M. DeMaria, K. Musgrave, J. Kaplan, C. M. Rozoff, J. P. Kossin and C. S. Velden,
2011: Improvements to statistical intensity forecasts. Proceedings, *65th Interdepartmental
Hurricane Conference*, Miami, FL, Off. Fed. Coord. Meteor. Serv. Supp. Res., Sess. 11.03,
<http://www.ofcm.gov/ihc11/Presentations/Session11/>.

Lander, M.A., 1994: Description of a monsoon gyre and its effects on the tropical cyclones in the
western North Pacific during August 1991. *Wea. Forecasting*, **9**, 640-654.

Lander, M.A., 1996: Specific tropical cyclone track types and unusual tropical cyclone motions
associated with a reverse-oriented monsoon trough in the western North Pacific. *Wea.*
Forecasting, **11**, 170–186.

Molinari, J., K. Lombardo, and D. Vollaro, 2007: Tropical cyclogenesis within an equatorial
Rossby wave packet. *J. Atmos. Sci.*, **64**, 1301-1317.

Molinari, J., and D. Vollaro, 2012: A subtropical cyclonic gyre associated with interactions of
the MJO and the midlatitude jet. *Mon. Wea. Rev.*, **140**, 343-357.

- Molinari, J., and D. Vollaro, 2013: What percentage of western north Pacific tropical cyclones form within the monsoon trough? *Mon. Wea. Rev.*, **141**, 499-505.
- Raymond, D.J., 1992: Nonlinear balance and potential-vorticity thinking at large Rossby number. *Quart. J. Roy. Meteor. Soc.*, **118**, 987-1016.
- Reasor, P.D., M. D. Eastin, and J. F. Gamache, 2009: Rapidly intensifying Hurricane Guillermo (1997). Part I: Low-wavenumber structure and evolution. *Mon. Wea. Rev.*, **137**, 603-631.
- Simmons A., S. Uppala, D. Dee, and S. Kobayashi, 2007: ERA-Interim: New ECMWF reanalysis products from 1989 onward. *ECMWF Newsletter*, **110**, 13 pp.
- Wu, L., H. Zong, and J. Liang, 2011: Observational analysis of sudden tropical cyclone track changes in the vicinity of the East China Sea. *J. Atmos. Sci.*, **68**, 3012–3031.
- Wu, L., H. Zong, and J. Liang, 2013a: Observational analysis of tropical cyclone formation associated with monsoon gyres. *J. Atmos. Sci.*, **70**, 1023-1034.
- Wu, L., Z. Ni, J. Duan, and H. Zong, 2013b: Sudden tropical cyclone track changes over the western North Pacific: A composite study. *Mon. Wea. Rev.*, **140**, 2597-2610.

Table 1. Sequence of tropical cyclone events in real time during 28 July – 4 August 1989. All warnings were issued by the Joint Typhoon Warning Center (JTWC). TCFA refers to Tropical Cyclone Formation Alert, indicating the likelihood that a tropical cyclone formation will occur within 24 hours.

TIME	EVENT
1200 UTC 28 July	Gyre formation
29 and 30 July	Warning on monsoon gales
0950 UTC 29 July	TCFA on future TS Ken
0400 UTC 30 July	Tropical depression (future Ken) declared
0600 UTC 30 July	TS Ken named
0000 UTC 31 July	TS Ken mislocated 465 km SE of actual position
0000 UTC 31 July	Last warning on TS Ken
0025 UTC 31 July	Remains of Ken still show a sheared TS on visible images
0600 UTC 31 July	TCFA on future TS Lola
1030 UTC 31 July	TS Lola named
1200 UTC 31 July	Lola expected to move northwest of Okinawa
0000 UTC 1 August	Lola turns south of Okinawa
0600-1800 UTC 1 August	Lola becomes almost stationary
0000 2 August	Lola moves northwestward
0000 4 August	Lola makes landfall in China

Table 2. Six-hourly evolution in TS Ken-Lola of maximum wind speed (kt; from JTWC post-season analysis); ambient vertical wind shear direction and magnitude (m s^{-1}), calculated following Corbosiero and Molinari (2003); underlying sea surface temperature (SST); and mean 1000-200 hPa wind in a 500-km radius around the storm.

DATE	MAX WIND (kt)	AMBIENT SHEAR (DEG @ m s^{-1})	SST (°C)	MEAN FLOW (DEG @ m s^{-1})
0600 UTC 29 JUL	20	037°@7.1	29.0	235°@3.3
1200 UTC 29 JUL	25	006°@8.8	28.7	228°@3.0
1800 UTC 29 JUL	25	005°@5.8	28.4	226°@4.9
0000 UTC 30 JUL	30	318°@5.6	27.9	214°@5.8
0600 UTC 30 JUL	45	257°@5.0	27.1	211°@7.1
1200 UTC 30 JUL	45	274°@6.1	26.5	174°@8.4
1800 UTC 30 JUL	45	231°@6.6	26.8	159°@6.4
0000 UTC 31 JUL	45	233°@7.2	27.1	126°@5.4
0600 UTC 31 JUL	50	229°@5.6	27.3	087°@5.4
1200 UTC 31 JUL	50	276°@4.8	28.2	069°@6.9
1800 UTC 31 JUL	50	255°@4.6	28.3	053°@4.6
0000 UTC 1 AUG	50	247°@3.6	28.5	046°@3.0
0600 UTC 1 AUG	50	196°@7.1	28.6	013°@1.4
1200 UTC 1 AUG	45	218°@8.4	28.6	043°@0.6
1800 UTC 1 AUG	40	201°@6.8	28.6	249°@1.1
0000 UTC 2 AUG	40	202°@6.4	28.6	194°@1.4
0600 UTC 2 AUG	45	187°@12.1	28.3	156°@1.8
1200 UTC 2 AUG	45	205°@11.6	28.0	117°@3.4
1800 UTC 2 AUG	45	188°@7.9	27.8	119°@5.1
0000 UTC 3 AUG	50	189°@6.8	27.4	118°@5.8
0600 UTC 3 AUG	50	168°@6.3	26.8	122°@5.8
1200 UTC 3 AUG	50	193°@7.2	26.2	110°@6.2
1800 UTC 3 AUG	45	192°@5.3	25.6	114°@6.4

FIGURE CAPTIONS

Figure 1. Infrared satellite image with surface winds from coastal stations, ships, and buoys, shown every 6 hours. Magenta wind barbs exceed gale force, while yellow barbs are below gale force. The post-season track from JTWC is shown in red, with the hurricane symbol indicating the position of TS Ken-Lola at each time. (a)-(d): 29 July; (e)-(h): 30 July; (i)-(l): 31 July. Long barb = 5 m s^{-1} ; short barb 2.5 m s^{-1} .

Figure 2. Once daily relative vorticity (hatching) and wind (vectors) at 850 hPa, plotted over infrared satellite images. (a) 0000 UTC 29 July; (b) 0000 UTC 30 July; (c) 0000 UTC 31 July; (d) 0000 UTC 1 August. Vorticity shading begins at $5 \times 10^{-5} \text{ s}^{-1}$, in increments of $5 \times 10^{-5} \text{ s}^{-1}$. Upper-case letters refer to individual vorticity maxima. The hurricane symbol indicates the location of Ken-Lola.

Figure 3. As in Fig. 2, but for 500 hPa temperature fields (contours; increment 0.5K) and 500 hPa wind (vectors). “W” and “C” refer to temperature maxima and minima.

Figure 4. As in Fig. 2, but for 200 hPa height (contours; increment 20 m) and winds. The L’s refer to 200 hPa height minima.

Figure 5. As in Fig. 2, but for 500 hPa relative humidity (yellow stippling: $> 60\%$; blue stippling: $< 40\%$) and winds.

Figure 6. Evolution of the location of the 1000 hPa (red) and 200 hPa (blue) height minima with respect to the midpoint between them, following the procedures of Holland and Lander (1993). Values extend from 1200 UTC 29 July (large circles) to 0600 UTC 1 August, every 6 hours. Range rings (km) represent the distance from the midpoint, so the actual distance between the 1000 and 200 hPa lows is double the range ring value.

Figure 7. 500 hPa temperature fields (contours; increment 0.5K) and 500 hPa wind (vectors) on 31 July, plotted over infrared satellite images. (a) 0000 UTC; (b) 0600 UTC; (c) 1200 UTC; (d) 1800 UTC.

Figure 8. Top panels: 500 hPa temperature (contours; increment 0.5K) and 500 hPa wind (vectors) at (a) 0000 UTC 2 August; and (b) 0000 UTC 3 August. Bottom panels: 200 hPa height (contours; increment 20 m) at (c) 0000 UTC 2 August; and (d) 0000 UTC 3 August. “H” and “L” refer to 200 hPa height maxima and minima.

Figure 9. Annotated JTWC post-season track of Ken/Lola, with shaded SST ($^{\circ}$ C) averaged for the time period of 27 July – 2 August 1989.

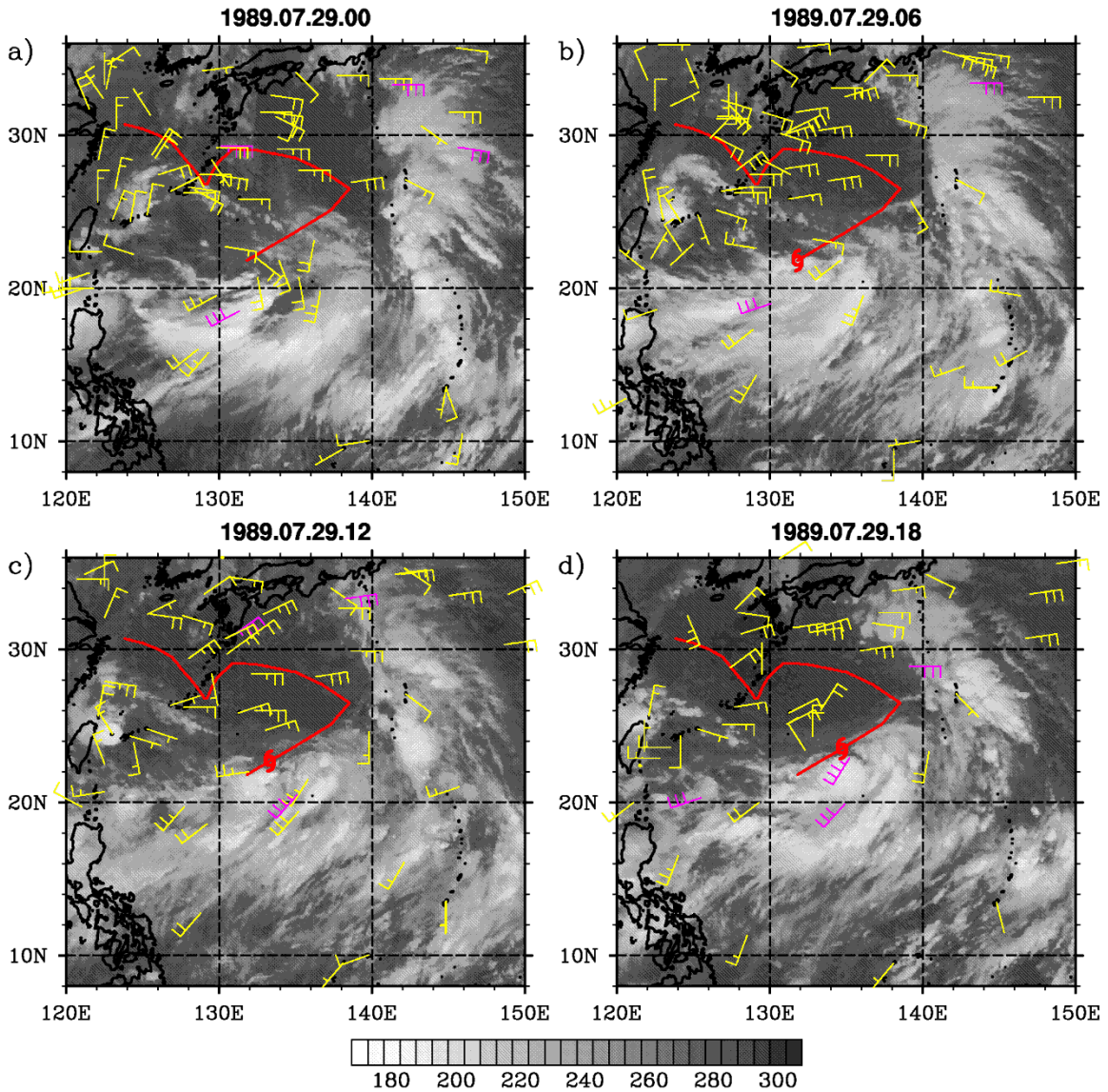


Figure 1. Infrared satellite image with surface winds from coastal stations, ships, and buoys, shown every 6 hours. Magenta wind barbs exceed gale force, while yellow barbs are below gale force. The post-season track from JTWC is shown in red, with the hurricane symbol indicating the position of TS Ken-Lola at each time. (a)-(d): 29 July; (e)-(h): 30 July; (i)-(l): 31 July. Long barb = 5 m s^{-1} ; short barb 2.5 m s^{-1} .

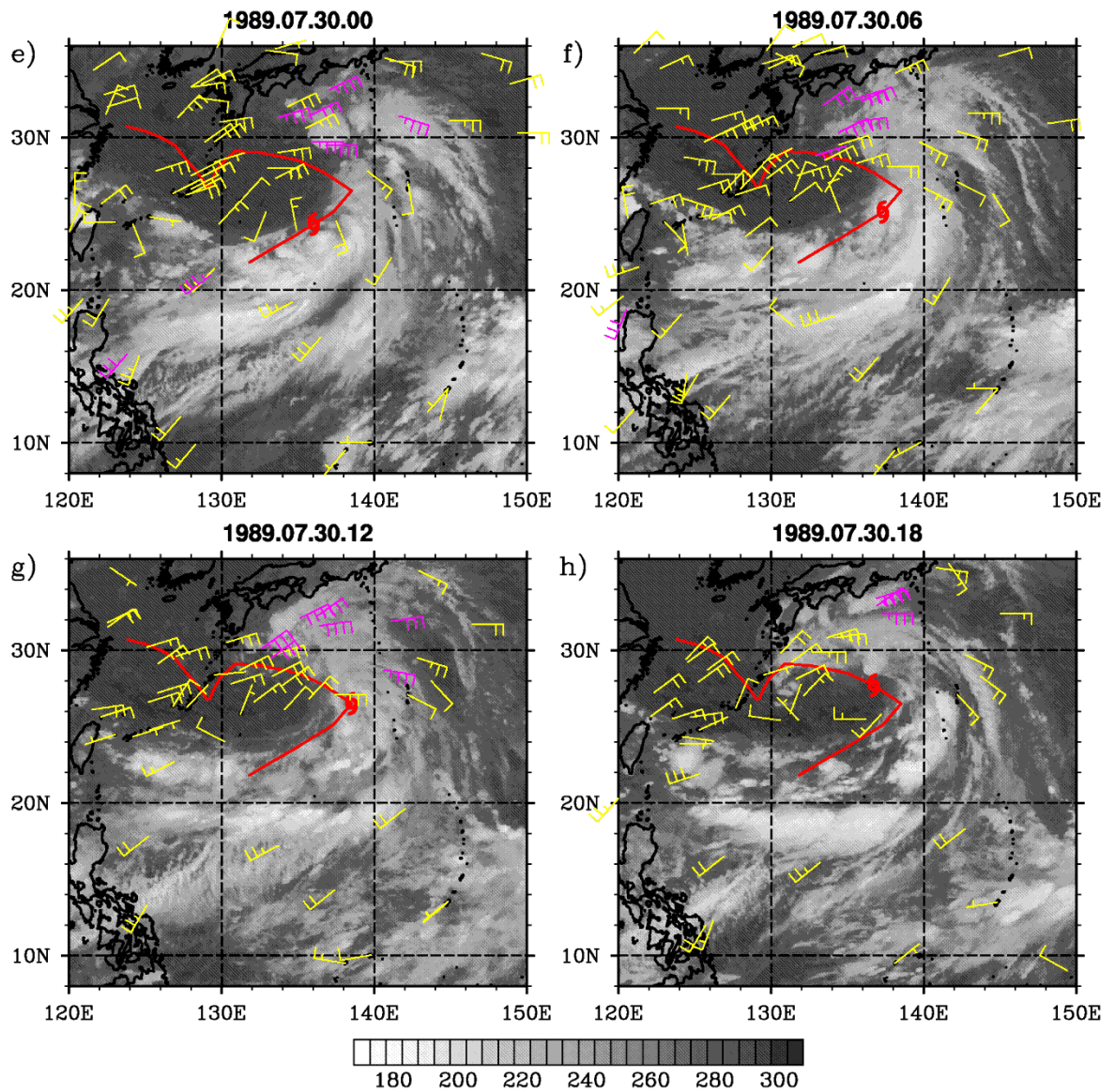


Figure 1 (e-h).

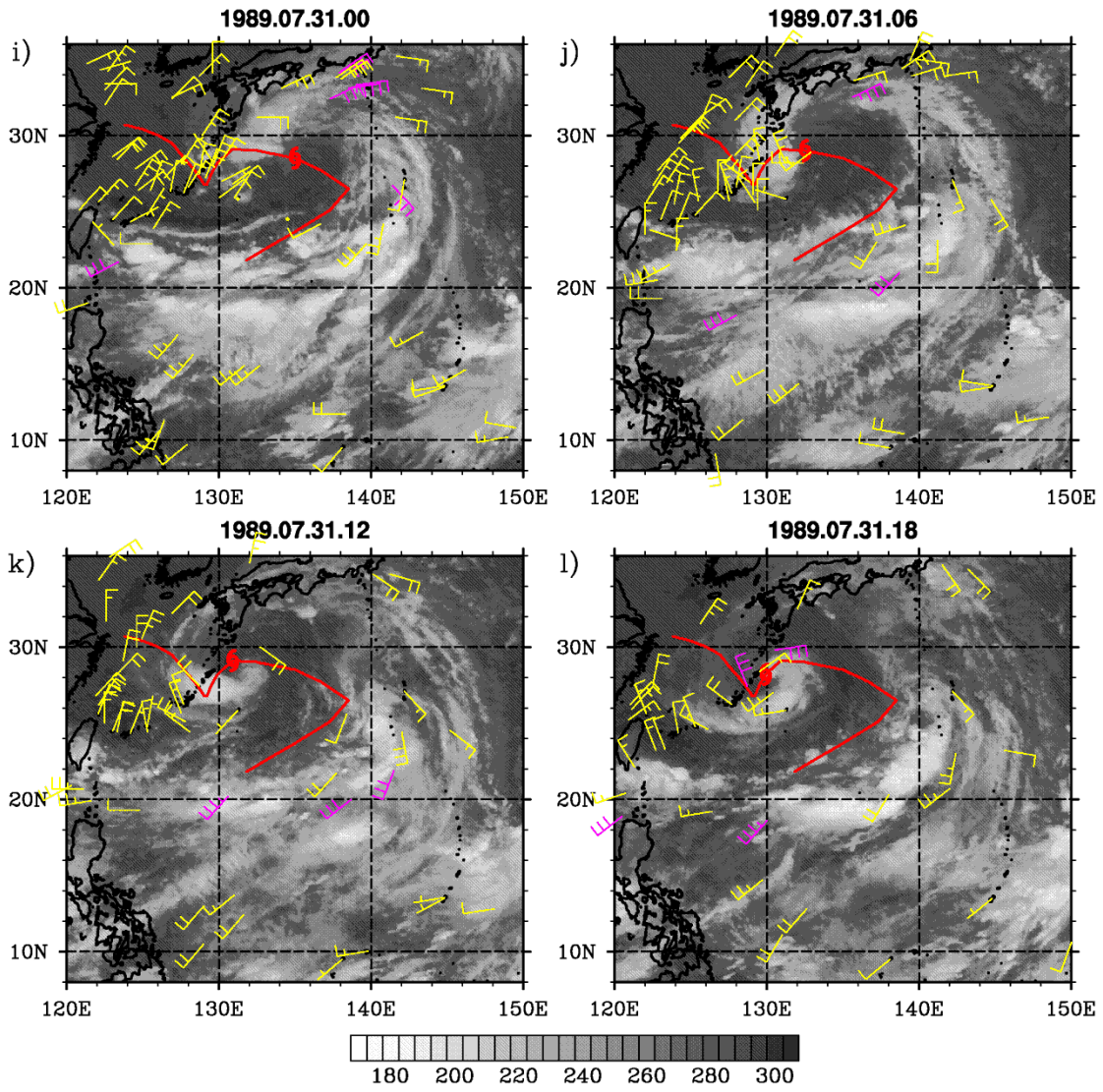


Figure 1 (i-l)

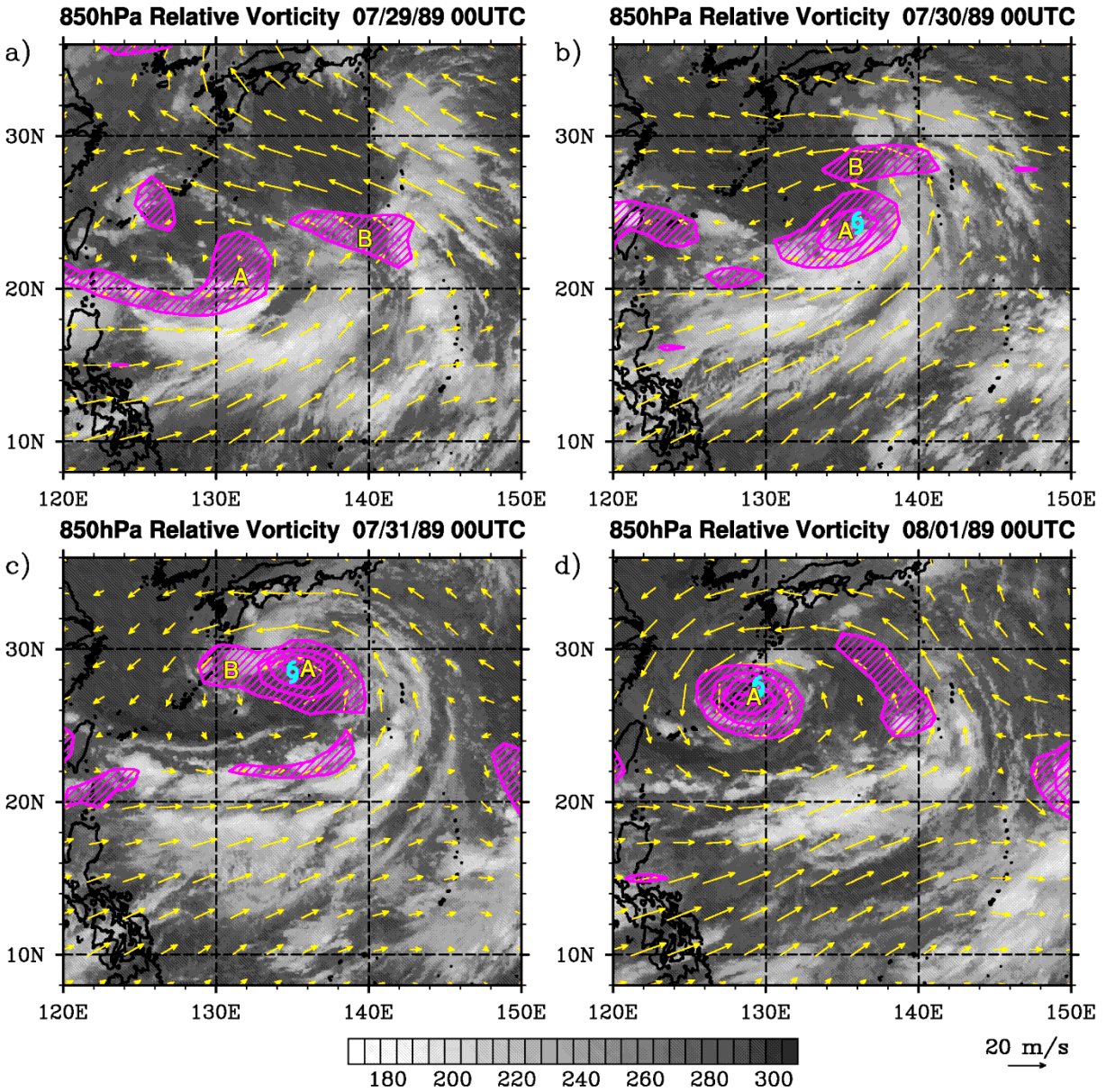


Figure 2. Once daily relative vorticity (hatching) and wind (vectors) at 850 hPa, plotted over infrared satellite images. (a) 0000 UTC 29 July; (b) 0000 UTC 30 July; (c) 0000 UTC 31 July; (d) 0000 UTC 1 August. Vorticity shading begins at $5 \times 10^{-5} \text{ s}^{-1}$, in increments of $5 \times 10^{-5} \text{ s}^{-1}$. Upper-case letters refer to individual vorticity maxima. The hurricane symbol indicates the location of Ken-Lola.

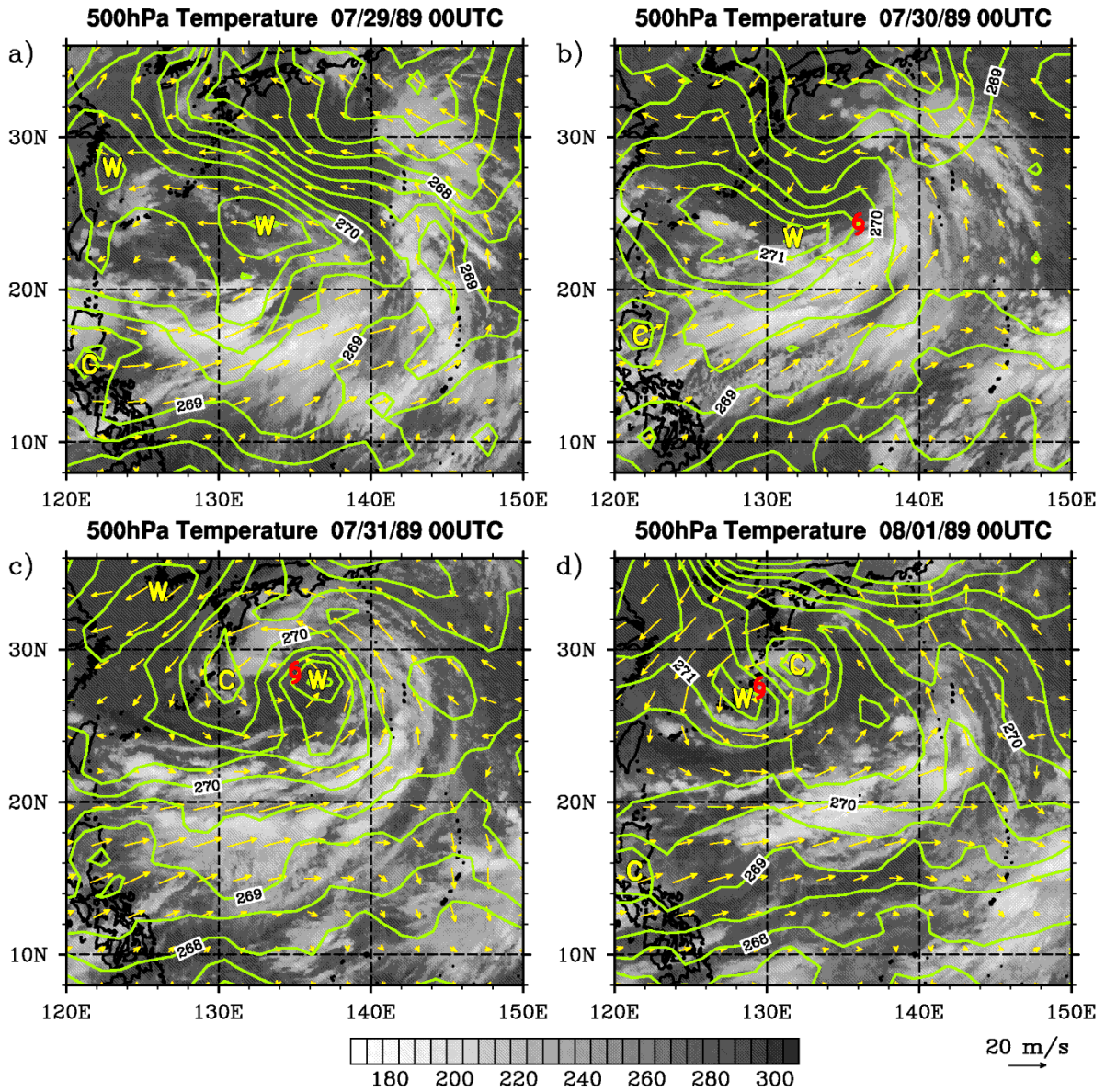


Figure 3. As in Fig. 2, but for 500 hPa temperature fields (contours; increment 0.5K) and 500 hPa wind (vectors). “W” and “C” refer to temperature maxima and minima.

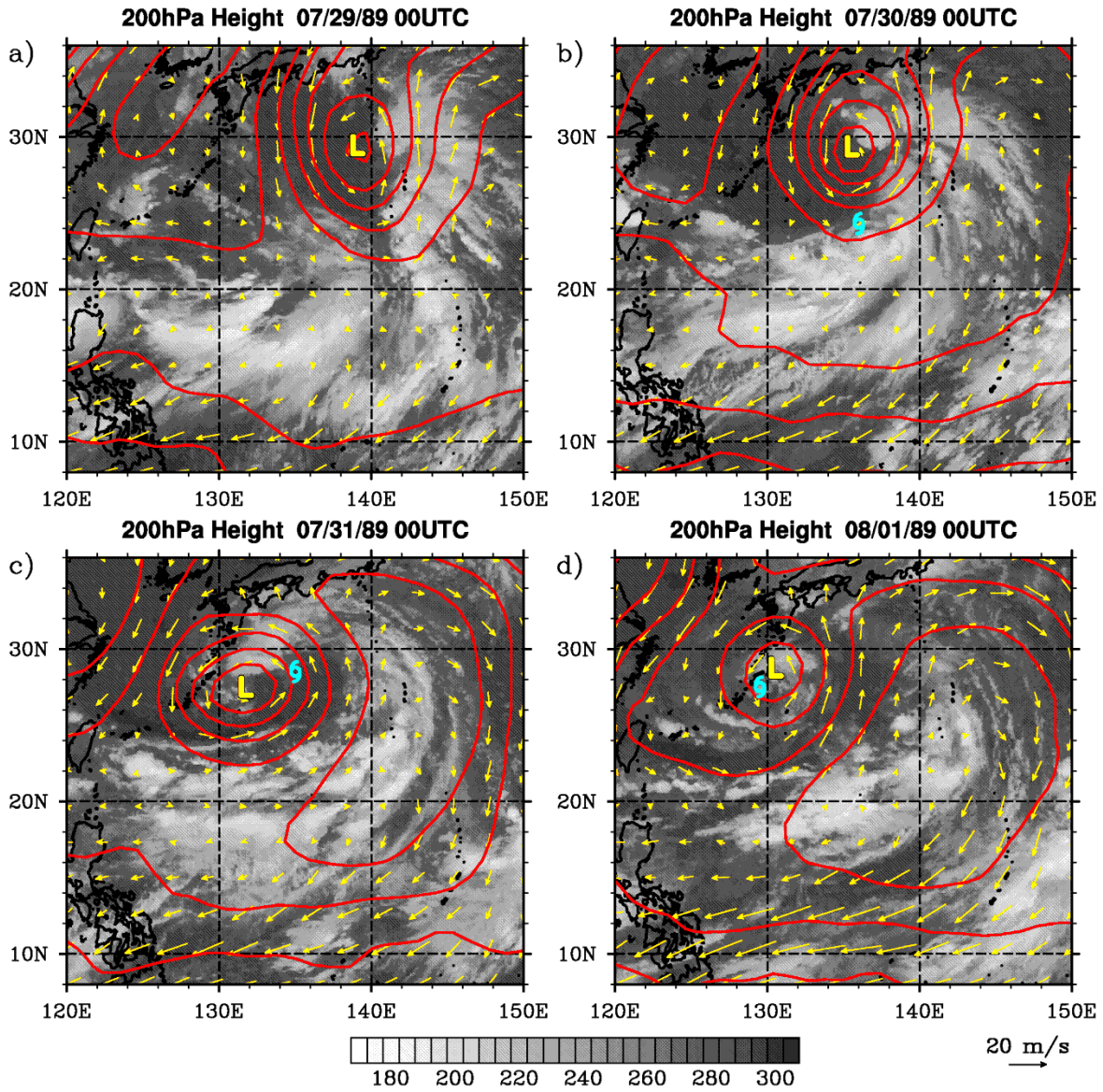


Figure 4. As in Fig. 2, but for 200 hPa height (contours; increment 20 m) and winds. The L's refer to 200 hPa height minima.

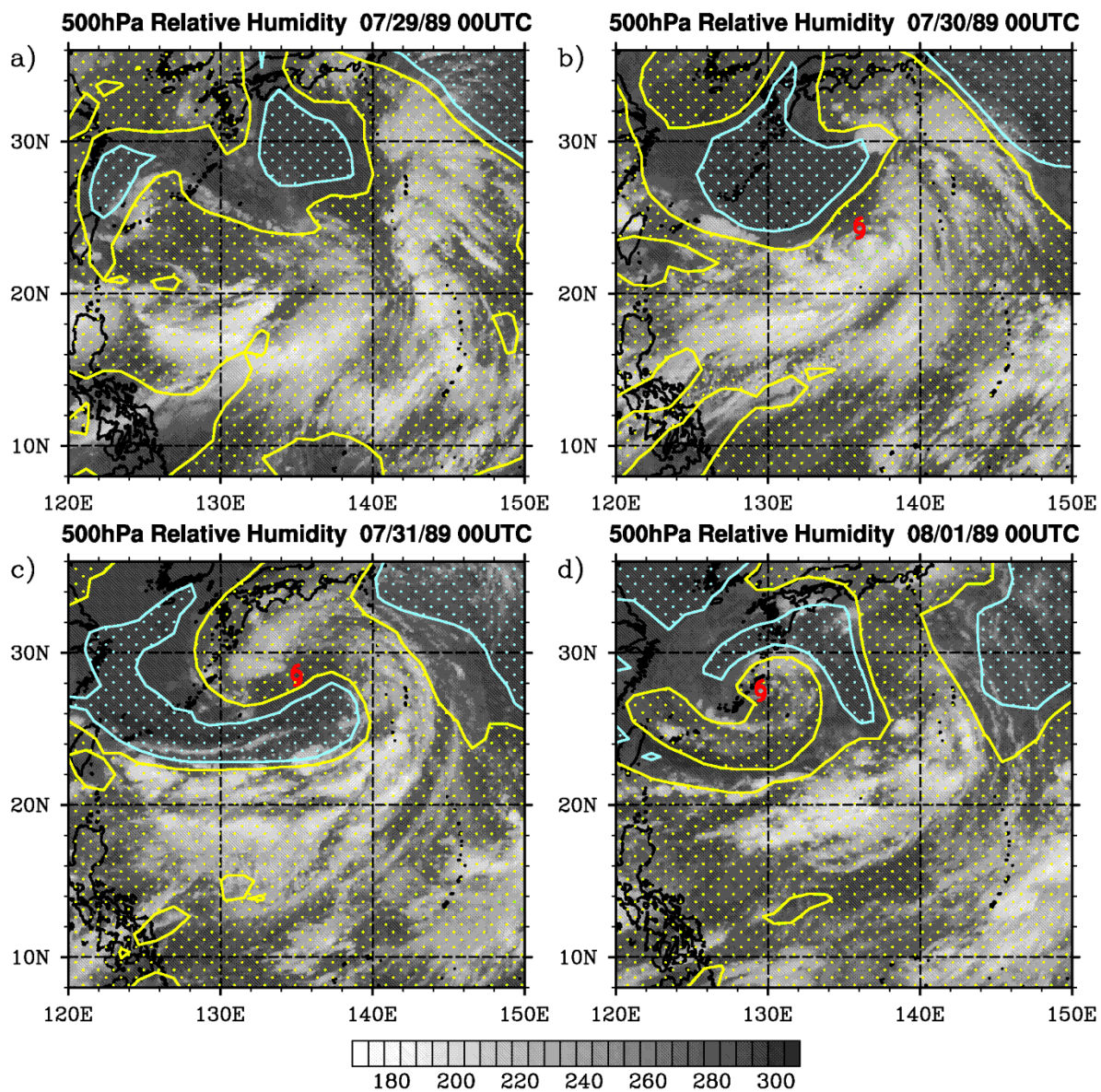


Figure 5. As in Fig. 2, but for 500 hPa relative humidity (yellow stippling: > 60%; blue stippling: < 40%) and winds.

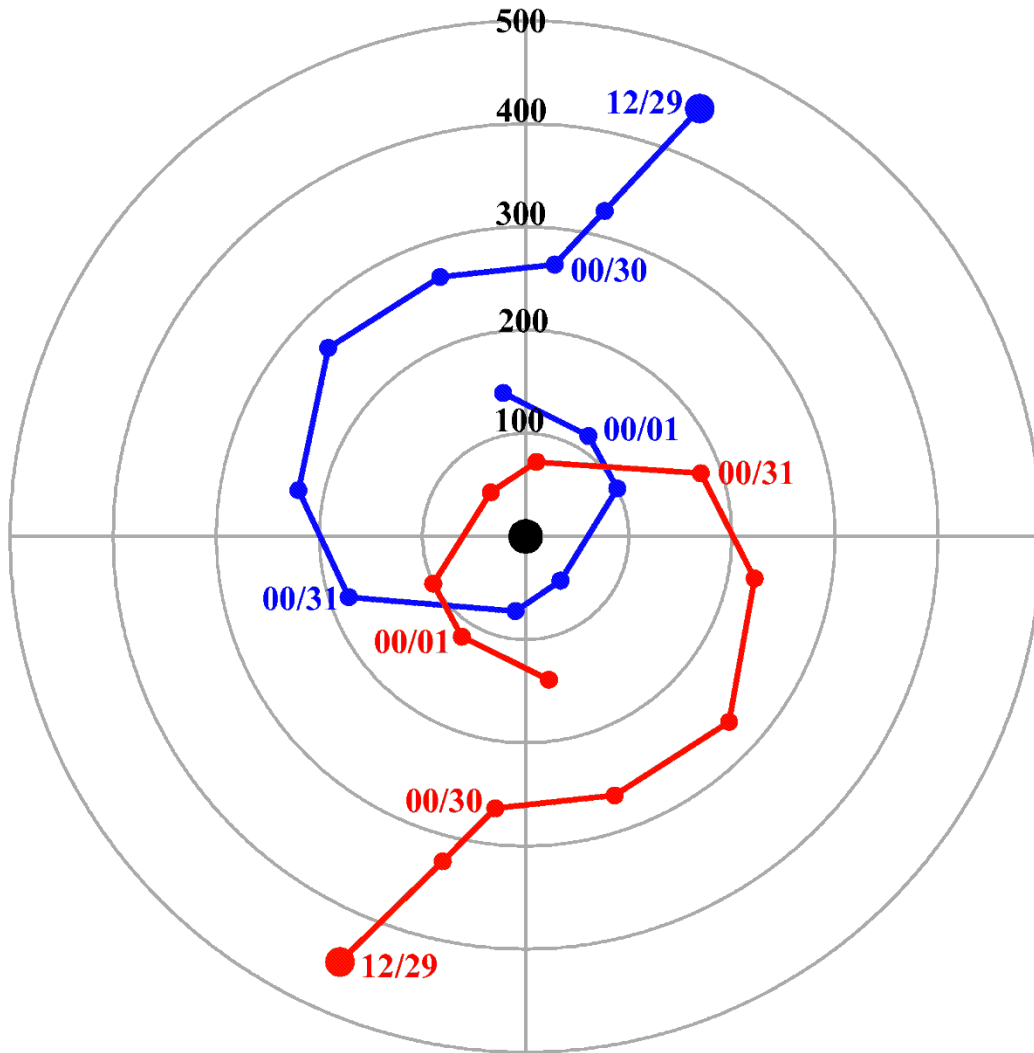


Figure 6. Evolution of the location of the 1000 hPa (red) and 200 hPa (blue) height minima with respect to the midpoint between them, following the procedures of Holland and Lander (1993). Values extend from 1200 UTC 29 July (large circles) to 0600 UTC 1 August, every 6 hours. Range rings (km) represent the distance from the midpoint, so the actual distance between the 1000 and 200 hPa lows is double the range ring value.

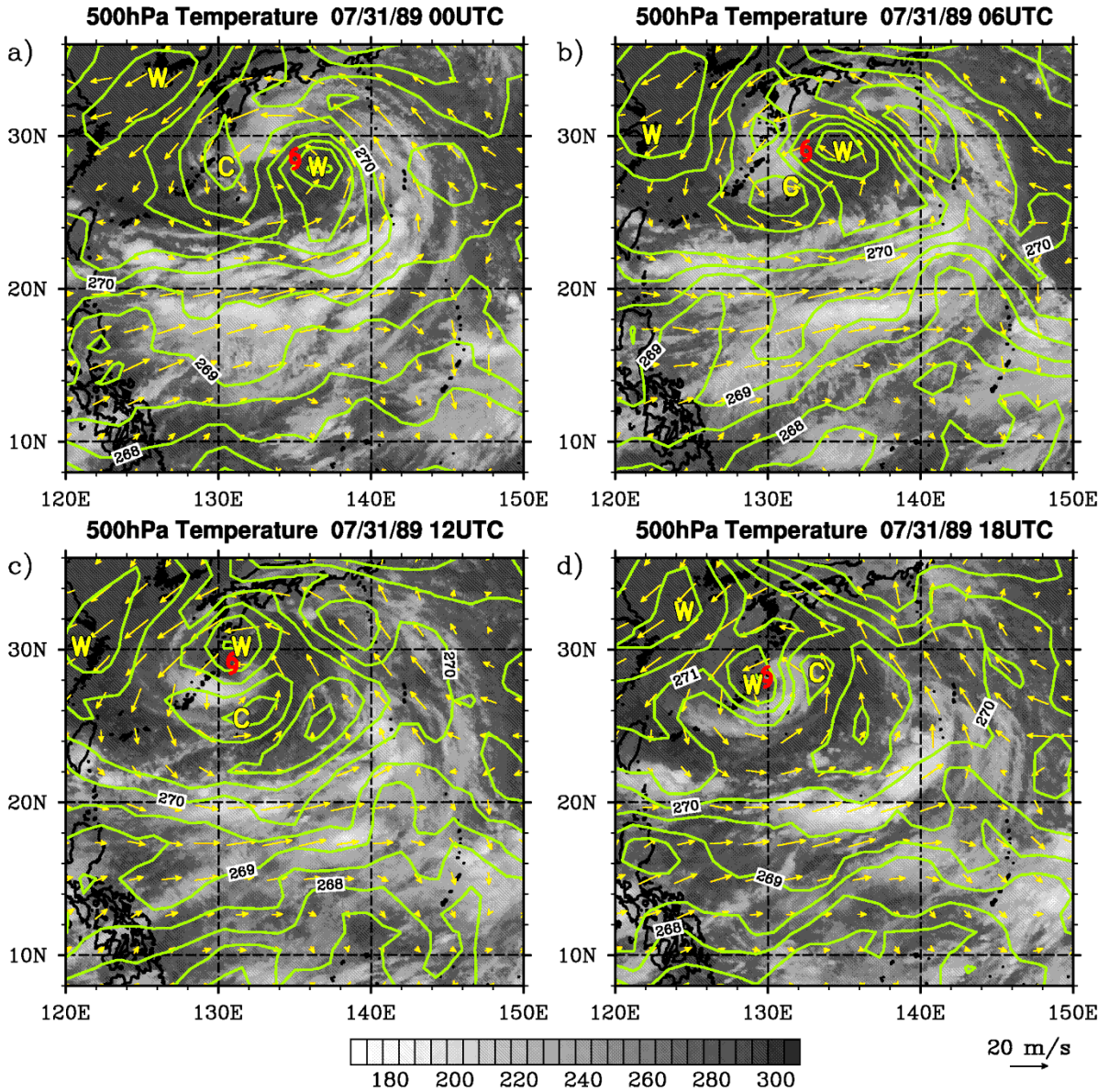


Figure 7. 500 hPa temperature fields (contours; increment 0.5K) and 500 hPa wind (vectors) on 31 July, plotted over infrared satellite images. (a) 0000 UTC; (b) 0600 UTC; (c) 1200 UTC; (d) 1800 UTC.

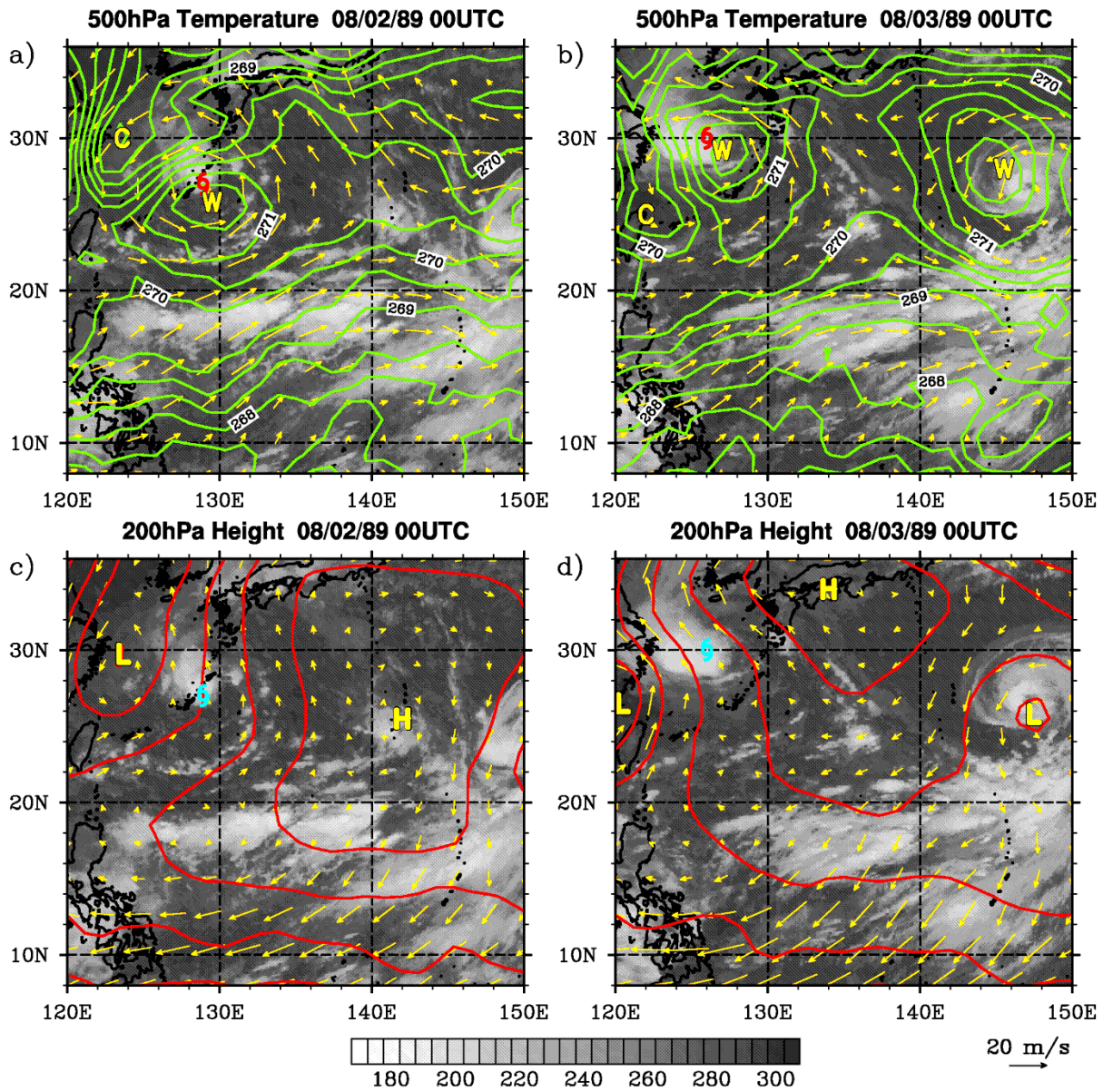


Figure 8. Top panels: 500 hPa temperature (contours; increment 0.5K) and 500 hPa wind (vectors) at (a) 0000 UTC 2 August; and (b) 0000 UTC 3 August. Bottom panels: 200 hPa height (contours; increment 20 m) at (c) 0000 UTC 2 August; and (d) 0000 UTC 3 August. “H” and “L” refer to 200 hPa height maxima and minima.

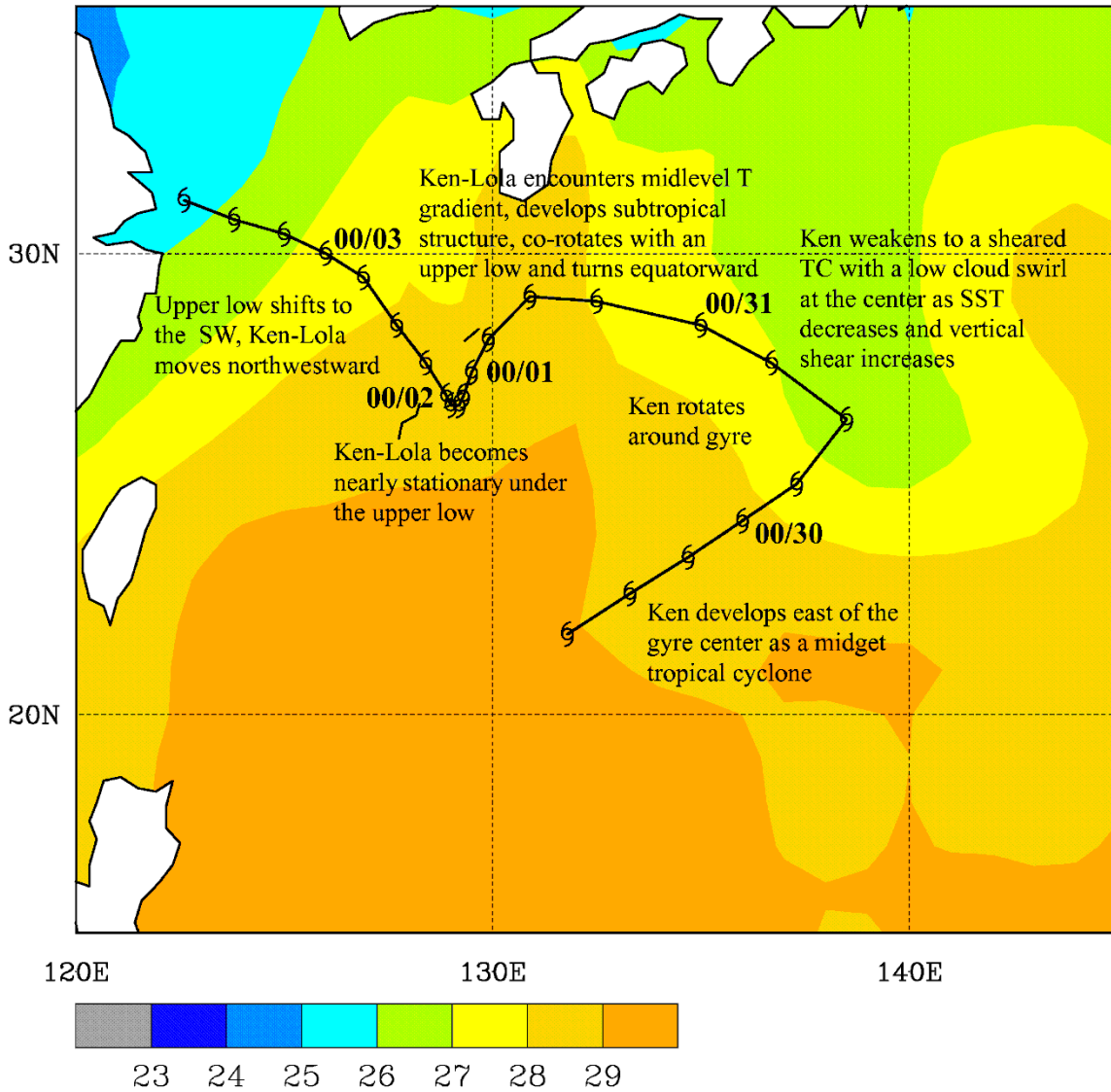


Figure 9. Annotated JTWC post-season track of Ken/Lola, with shaded SST ($^{\circ}\text{C}$) averaged for the time period of 27 July – 2 August 1989.